Mon. Not. R. Astron. Soc. **386,** 995–1012 (2008) doi:10.1111/j.1365-2966.2008.13083.x

A GLIMPSE of new and possible planetary nebulae at mid-infrared wavelengths

J. P. Phillips★ and G. Ramos-Larios

Instituto de Astronomía y Meteorología, Av. Vallarta No. 2602, Col. Arcos Vallarta, CP 44130 Guadalajara, Jalisco, Mexico

Accepted 2008 February 7. Received 2008 January 28; in original form 2007 December 19

ABSTRACT

We have undertaken a mid-infrared (MIR) search for new planetary nebulae (PNe) using the *Spitzer Space Telescope* GLIMPSE Galactic plane survey. This has involved searching extant GLIMPSE data products for morphologically appropriate structures, and investigating sources having *IRAS* colours similar to those of Galactic PNe. We have found 12 sources which have a high probability of being high-extinction PNe, and which possess MIR and *IRAS* colours, and shell morphologies similar to those of previously identified Galactic nebulae. Calibrated mapping of these structures and profiles in all four of the IRAC bands (3.6, 4.5, 5.8 and 8.0 μm) suggests that many (if not all) of the nebulae possess at least two primary structures: an interior high surface brightness shell, corresponding to what is probably the primary ionized zone, and a much weaker halo extending to very much greater distances from the nucleus. These latter regimes are particularly evident at longer MIR wavelengths (5.8 and 8.0 μm), and it is probable that they trace the nebular photodissociative regimes, where emission derives from small-grain continua and/or polycyclic aromatic hydrocarbon molecular bands. This latter behaviour has also been noted in previous analyses of Galactic PNe.

Key words: ISM: lines and bands – ISM: molecules – planetary nebulae: general – infrared: ISM.

1 INTRODUCTION

Various estimates have been quoted for the population of Galactic planetary nebulae (PNe), ranging from as low as $\sim 2 \times 10^3$ (Pottasch 1984) to of the order of 4.3×10^5 (Cahn & Kaler 1971), although most modern estimates would place the total at closer to $\approx (2 \pm 1) \times 10^4$ (see e.g. Peimbert 1990; Zijlstra & Pottasch 1991; Peimbert 1993; Phillips 2002; earlier values have been summarized by Phillips 1989). These estimates are an order of magnitude greater than the number of known PNe (2000–2500; see e.g. Parker et al. 2003), a disparity which is explicable in terms of various well-established observational causes. In the first place, surveys of PNe have usually been extremely patchy, with differing areas of the Galactic plane being surveyed to differing levels of completeness. This is partially attributable to the differing limiting sensitivities of photographic/spectral surveys, and the difficulty of identifying angularly compact sources and low surface brightness shells.

Perhaps more important than all these factors however, critical though they may be, is the difficulty of detecting low latitude sources in regimes where levels of extinction are high. The number densities of PNe increase almost exponentially with decreasing $|b|$ (see e.g. Perek & Kohoutek 1967; Phillips 2001), and a large fraction of PNe are located in regimes where extinctions are very large indeed. If one uses the line-of-sight Galactic extinction results of Schlegel, Finkbeiner & Davis (1998), for instance, then it is clear that the mean extinctions for $|l| < 50^\circ$, and $|b| < 1^\circ$ exceed $\langle A_V \rangle \sim 12.6$ mag. As would be expected, most observed PNe within this regime have values of A_V which are very much less (Phillips 2006a) and correspond to very much lower extinction foreground sources. It therefore follows that our sampling of these nebulae must be very partial indeed.

One way of overcoming these restrictions is by observing at wavelengths where levels of extinction are reduced. Galactic plane surveys at radio wavelengths, for instance, have identified several candidate PNe (CPNe) (e.g. Becker et al. 1994), although it is difficult to discriminate between PNe, H II regions, and young stellar objects (YSOs) using radio observations alone. Although ultracompact H II regions and PNe have differing distributions within the $F(5\,\mathrm{GHz})/F(1.4\,\mathrm{GHz})$–$T_\mathrm{B}(5\,\mathrm{GHz})$ plane, for instance, the differences are not sufficient to reliably discriminate between these differing types of source (e.g. Phillips 2007a,b,c,d).

An alternative and rather more promising possibility is to use surveys at infrared (IR) wavelengths, and several such surveys have been undertaken in the last twenty or so years. Thus, the recent 2MASS all-sky survey at J, H and K_S permitted many well known PNe to be mapped and investigated (e.g. Phillips & Ramos-Larios 2005, 2006, 2007; Ramos-Larios & Phillips 2005, 2006). Extinction within the longer wavelength K_S band is only ∼1/10th

★E-mail: jpp@astro.iam.udg.mx

of that in the visible, and this should also have permitted the detection of many more nebulae than are known at present. However, the sensitivity of the survey turned out to be too limited for this kind of work, and an unpublished analysis by one of us (jpp) failed to turn up many convincing sources.

The *IRAS* survey in the wavelength range 12–100 μm was, by contrast, much more penetrative, although the angular resolution was only ∼3.5 arcmin (see e.g. the *IRAS* Sky Atlas Explanatory Supplement at http://irsa.ipac.caltech.edu/IRASdocs/issa.exp.sup/). Although somewhat higher resolutions have been obtained for individual mapping programs (see e.g. Leene & Pottasch 1987, and also the HIRES programme described in http://irsa.ipac.caltech.edu/IRASdocs/hires_over.html, where resolutions of up to ∼1 arcmin have been achieved by using the maximum correlation method of Aumann, Fowler & Melnyk 1990), resolutions remain much too low to resolve most nebular structures. Nevertheless, various analyses of the point-source data base revealed several candidate PNe (e.g. Pottasch et al. 1988; Preite-Martinez 1988; Manchado et al. 1989; Garcia-Lario et al. 1990, 1997). These were identified, for the most part, on the basis of their $S(12\,\mu\mathrm{m})/S(25\,\mu\mathrm{m})$ and $S(60\,\mu\mathrm{m})/S(25\,\mu\mathrm{m})$ flux ratios, and we shall be returning to a discussion of these analyses later in Section 2.

Finally, the *Spitzer Space Telescope* now permits us to undertake mapping and spectroscopy between 3 and 180 μm (Werner et al. 2004), and with much higher sensitivities and spatial resolutions than was possible with *IRAS*. In particular, the Galactic Legacy Infrared Mid-Plane Survey Extraordinaire ('GLIMPSE'; see Benjamin et al. 2003) has mapped the Galactic plane within the latitude and longitude ranges $|b| \leqslant 1^\circ$, and $|l| = 10^\circ$–65°. The spatial resolution varied between 1.66 and 1.98 arcsec (Fazio et al. 2004), and the pointing accuracy was of the order of ∼0.3 arcsec. The IR camera was used to take 77 000 pointed observations, and produced 310 000 frames over a period of 400 h. These results were subsequently processed to yield the GLIMPSE Image Atlas, which contains $1643\farcm1 \times 2\farcm4$ mosaics in the four IRAC bands. These have isophotal wavelengths (and bandwidths) of 3.550 μm (0.75 μm), 4.493 μm (1.9015 μm), 5.731 μm (1.425 μm) and 7.872 μm (2.905 μm).

We have used the results of this survey to investigate the morphologies (and likely natures) of the CPNe, and to undertake an independent search for high-extinction PNe. We have found a total of 12 sources with appropriate morphologies, and far-IR (FIR) and mid-IR (MIR) colours similar to those of known PNe. The strength of the morphological and colour constraints makes it likely that they are previously unrecognized PNe.

2 SELECTION CRITERIA AND CANDIDATE SOURCES

The identification of sources as PNe is traditionally based upon a broad range of observational data, and takes account of the observed morphologies, spectral line ratios, central star characteristics and so forth (see e.g. Sabbadin, Minello & Bianchini 1977; Phillips 2004; Riesgo & López 2006; and general discussions in Pottasch et al. 1988; Kwok 2000). Many of these properties are unavailable for the sources to be identified below. Nevertheless, the evidence of *IRAS* and *Spitzer* MIR fluxes, and the high-resolution images to be presented here, enables one to assert that a very large proportion of our candidates are likely to be PNe.

We have used three main sets of procedures to identify high-extinction PNe.

2.1 Survey of the GLIMPSE Atlas

We have surveyed the entire GLIMPSE Atlas for likely nebular candidates (see Benjamin et al. 2003 for the seminal article on this Atlas; the high resolution (0.6 arcsec pixel^{-1}) data version is available at http://data.spitzer.caltech.edu/popular/glimpse/20070416_enhanced_v2/1.1x0.8_mosaics/). Specifically, the GLIMPSE team has provided individual, and slightly overlapping images of the ATLAS for each IRAC band, and for ranges of $\Delta l = 1\fdg1$ in Galactic longitude, and $\Delta b = 0\fdg8$ in Galactic latitude, leading to a total of 1344 plates for the four bands combined. Similarly, combined plates for all four of the IRAC bands have also been created, colour coded so as to discriminate between sources emitting preferentially at longer wavelengths (which appear red), or at intermediate and/or shorter wavelengths (which appear green or blue). We have surveyed these latter plates for the present analysis, wherein most ionized regions have a predominately white-red colouration.

This process was, inevitably, extremely time consuming, but permitted us to detect a range of possible compact and evolved PNe. Most of the compact nebulae were subsequently deleted from the sample, as described below, leaving a total of four sources which are likely to represent high-extinction PNe.

The criteria used to select the nebulae were relatively rigorous, and are detailed below.

(i) Sources were excluded if they were associated with extended longer filaments and webs of emission.

(ii) They were required to be far from other ionized 'bubbles' or structures.

(iii) They were required not to be part of, or apparently incorporated into H II regions, or more extended regions of star formation.

(iv) They were required to have morphologies typical of known (and 'standard') PNe. This will inevitably lead to the removal of any PN with non-standard appearance – particularly those with irregular structures. It should be added that where well-resolved IRAC imaging is available for known PNe (see e.g. Hora et al. 2004; Su et al. 2004; Cohen et al. 2005; Bernard-Salas et al. 2006; Hora et al. 2006; Kraemer et al. 2006; Ueta 2006; Su et al. 2007; Kwok et al. 2008; Phillips & Ramos-Larios 2008), then morphologies at MIR wavelengths are very closely similar to those in the visible – there appear to be few (if any) cases where source morphologies vary with wavelength, although there may, in some cases, be differences in structure and shell size. It is therefore unlikely that there are PNe at MIR wavelengths with structures differing from those with which we are familiar.

(v) The sources were, for the most part, required to have dimensions which were greater than ∼10 arcsec. Although several more compact nebulae were identified in this survey, and fulfilled most of the criteria for selection as PNe (the sources were roughly circular, not associated with H II regions etc.), the morphologies of the sources were not very well established, and they could have been confused with other forms of stellar mass-loss.

(vi) If *IRAS* photometry existed for the sources, then they were required to have $F(25\,\mu\mathrm{m})/F(12\,\mu\mathrm{m})$ and $F(60\,\mu\mathrm{m})/F(25\,\mu\mathrm{m})$ flux ratios consistent with the PNe criteria of Pottasch et al. (1988). This turned out to be one of the most stringent criteria for eliminating sources, and resulted, in combination with certain of the previous criteria, in the removal of ∼73 per cent of nebulae identified as potential PNe. The fraction of sources with morphologies similar to

PNe, but rejected according to all of the previous criteria combined, is of the order of ∼97 per cent.

(vii) The sources were finally required to have MIR colours typical of PNe. Although we initially took this to be an important criterion in the selection of our sources, it turned out that all of the sources identified using criteria (i)–(vii) were located in the appropriate colour range. We also later determined that contrary to the stated results of certain previous investigations (see e.g. Cohen et al. 2007b), the PNe colour range did not differ very greatly from that of H II regions (see our discussion later this section). It therefore appears that this particular criterion may turn out to be redundant.

This is a very conservative set of criteria, and means that many potential (or real) PNe may have been eliminated from our survey. Such criteria also tend, for the most part, to eliminate structures close to $b = 0^\circ$ – including sources which would normally be regarded as morphologically suggestive.

Images of the sources thus selected are presented in Fig. 3 (see later), whilst details of positions, *IRAS* fluxes, and MIR magnitudes are listed in Table 1 (the sources are identified as series 1 nebulae in column 6). Note, in this respect, that the flux quality factor FQ (column 11) is an *IRAS* designated code, and flags whether the measurements are of a high quality (3), moderate quality (2), or simply represent an upper limit flux (1). The four numbers in the column refer consecutively to the 12-, 25-, 60- and 100-μm fluxes. We have also given two sets of dimensions at 8 μm, one corresponding to the full width at half-maximum (FWHM) of the nuclei, determined using Gaussian deconvolution (see column 16), and the other to the maximal dimensions of the envelopes (in column 17). Profiles through the sources are illustrated in Figs 5(a), (b), 7(a), (b), 10 and 14 (see later), wherein we have averaged emission over slices of width 3–4 pixels (see details in the captions to these figures), equivalent to angular widths of between 1.8 and 2.4 arcsec. These profile widths are comparable to the spatial resolution of the GLIMPSE survey (see Section 1).

Finally, combined RGB (red–green–blue) images are presented in Fig. 3 (later). In these latter cases, the colour designations are as detailed in the caption to the figure, although it is generally the case that red colours represent longer wavelengths (and correspond mostly to the 8-μm imaging), whilst blue colours correspond to the shorter 4.5-μm channel.

We have, finally, also provided four-band contouring of the sources in Figs 4, 6, 9 and 13 (see later). In these latter cases, fluxes E_n corresponding to the differing contour levels n are given through

$$E_n = A \times 10^{(n-1)\Delta C} - B \ \mathrm{MJy\ sr^{-1}}, \quad (1)$$

where A is a constant, $n = 1$ corresponds to the lowest (i.e. the outermost) contour level, B is the background, and ΔC is the logarithmic separation between contours. The parameters A, ΔC and B are specified in the captions to the figures. The background term is of most importance at 8 μm, and is found, for the most part, to be reasonably uniform. It consists primarily of instrumental noise, large-scale emission from diffuse interstellar gas and H II regions, and (particularly at shorter wavelengths) a component arising from field stars. This latter contribution leads to a veil of weak point source functions which may, in certain cases, be almost spatially continuous – the individual PSFs overlap within the relevant image planes.

The MIR magnitudes were determined by employing circular, elliptical, polygonal or rectangular apertures, and fitting these to the observed source structures. The fluxes measured in these apertures

Table 1. List of newly identified, and spatially resolved PNe.

No.	G.C.	α (2000)	δ (2000)	IRAS	Series	F(12 μm) (Jy)	F(24 μm) (Jy)	F(60 μm) (Jy)	F(100 μm) (Jy)	FQ	[3.6] (mag)	[4.5] (mag)	[5.8] (mag)	[8.0] (mag)	FWHM(nuc) (arcsec)	θ(outer) (arcsec)
1	010.211 +0.429	18 06 36.18	−19 53 47.0	18036−1954	1	1.549	9.733	34.45	406.6	3331	7.45	6.93	5.15	3.29	21	53
2	010.393 +0.538	18 06 34.37	−19 41 04.8	18036−1941	1	3.08	28.11	102.1	160.9	3333	7.99	7.57	5.64	3.86	3.7	56
3	020.468 +0.679	18 25 58.08	−10 45 28.7	18231−1047	2	3.56	12.41	15.3	227	1331	10.13	9.23	8.52	6.25	2.3	13.8
4	031.662 +0.366	18 47 48.88	−00 57 48.0	18452−0191	2	4.28	16.42	32.11	437	3331	9.30	8.06	6.29	4.48	1.2	36
5	032.990 +0.040	18 51 24.07	+00 04 11.2	18488+0000	1	8.582	39.56	43.01	92.06	3333	8.24	7.48	5.04	3.36	–	50
6	037.277 −0.227	19 00 10.88	+03 45 46.9	18576+0341	3	58.48	425	274.7	1660	3331	6.12	5.42	3.41	–	4.2	14.5
7	049.695 +0.864	19 19 33.61	+15 16 46.9	19172+1511	1	1.663	24.48	79.98	63.09	3333	8.85	8.49	6.12	4.32	1.1	50
8	296.320 +0.682	11 55 38.03	−61 28 16.9	11531−6111	2	0.29	2.58	1.55	50	1331	10.24	9.57	8.65	6.80	2.1	12.6
9	322.208 −0.743	15 24 24.07	−57 46 21.2	15204−5735	2	1.63	5.84	10.14	174	1331	10.09	9.11	8.11	6.34	1.9	13.2
10	327.830 −0.888	15 57 21.10	−54 30 46.0	15534−5422	2	1.25	9	11.91	353	3321	9.89	9.22	7.82	5.79	2.6	16.8
11	342.226 −0.380	16 56 33.95	−43 46 14.9	16529−4341	2	1.48	22.33	21.71	343	3331	9.32	8.19	7.97	6.24	3.1	19.8
12	346.683 +0.855	17 05 59.94	−39 29 41.0	17025−3925	2	0.52	4.88	13.69	57.3	1331	12.54	11.48	10.34	8.35	3.5	12.6

were then corrected for sky background, and for the fluxes arising from contaminating field and central stars. Complex scattering of light in the array focal planes requires the correction of photometry taken with large aperture measurements (see e.g. the SSC web page at http://ssc.spitzer.caltech.edu/IRAC/calib/extcal/) – an effect which is particularly important at 5.0 and 8.0 μm, and may arise due to scattering in an epoxy layer between the detector and multiplexer (Cohen et al. 2007a). We have taking this into account by respectively adding +0.10 mag, +0.07 mag, +0.40 mag and +0.33 mag to the results at 3.6, 4.5, 5.8 and 8.0 μm.

Finally, the magnitudes of the sources were evaluated from the observed fluxes, and by using the most recent Vega calibration due to Reach et al. (2005).

The resulting *Spitzer* [3.6] − [4.5]/[5.8] − [8.0] colour diagram is illustrated in Fig. 1 (upper panel), where we also show trends determined for other sources in our study (see Sections 2.2 and 2.3),

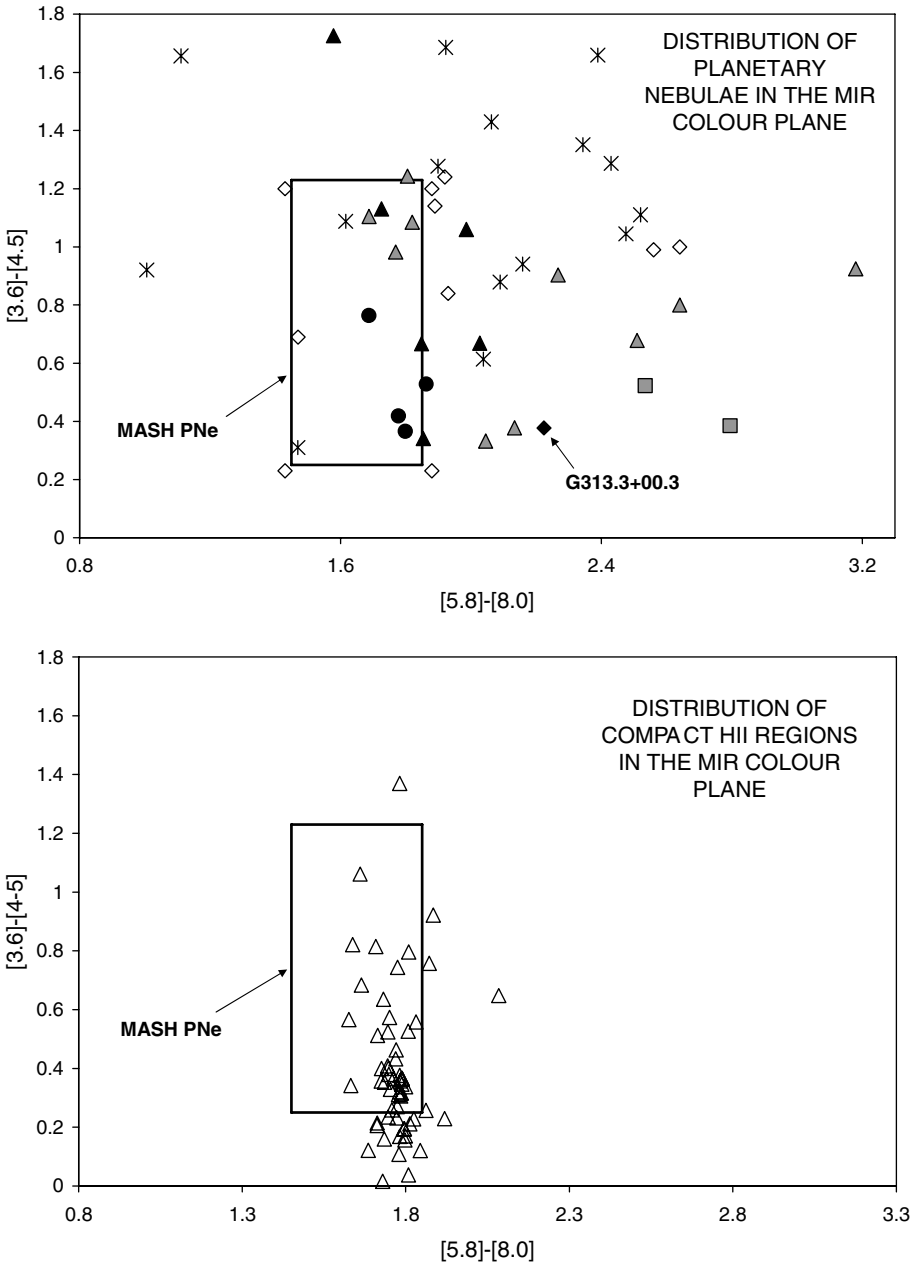

Figure 1. Upper panel: Positions of newly identified PNe within the [3.6] − [4.5]/[5.8] − [8.0] colour plane, where filled circles correspond to nebulae detected through a survey of the GLIMPSE data products, as described in Section 2.1; filled triangles are spatially resolved nebulae identified using the GLIMPSE survey, and the catalogue of Preite-Martinez (1988) (Section 2.2); grey triangles represent the corresponding unresolved Preite-Martinez sources; and finally the two grey squares correspond to unresolved 5-GHz/*IRAS* sources, as described in Section 2.3. The filled lozenge corresponds to the probable PNe G313.3+00.3 discovered by Cohen et al. (2005). We have also illustrated various known Galactic PNe, including those investigated by Phillips & Ramos-Larios (2008) (stars), Hora et al. (2004) (open lozenges) and Cohen et al. (2007b) (the rectangle indicating the location of MASH PNe). Lower panel: Positions of 60 H II regions within the MIR colour plane. Note how the H II regions occupy a more restrictive range of colours [5.8] − [8.0], but strongly overlap the regime of the PNe.

and for various Galactic PNe (taken from Hora et al. 2004; Cohen et al. 2007b; Phillips & Ramos-Larios 2007). One of the sources corresponds the *Spitzer*-detected PN G313.3+00.3 of Cohen et al. (2005).

In addition to the distribution of PNe illustrated in Fig. 1, we have recently become aware of an independent SAGE survey of LMC PNe (Hora et al. 2008). This confirms that the majority of LMC sources fall within the same regime of the [3.6] − [4.5]/[5.8] − [8.0] colour plane. Although some ∼15 per cent of the nebulae also fall outside of this range, most of these extraneous sources have indices [3.6] − [4.5] and [5.8] − [8.0] which are smaller, in many cases approaching ∼0. It is therefore likely that many of these nebulae are dominated by central star emission, as is the case for comparable sources within the $J - H/H - K_S$ colour plane (see e.g. Phillips & Ramos-Larios 2005). By contrast, the colours illustrated in Fig. 1 are largely free of this bias, and central star contributions are small.

A similar log(S(60 μm)/S(25 μm))–log(S(25 μm)/S(12 μm)) *IRAS* colour diagram is shown in Fig. 2, where in this case the comparative results for PNe, H II regions, stars, OH/IR stars and galaxies are taken from Pottasch et al. (1988). We also show the results for all of our survey nebulae (listed in Table 1), and various unresolved sources whose morphologies are undefined (grey symbols; see also our discussions in Sections 2.2 and 2.3 below). It is clear that the sources detected through the present GLIMPSE survey are located within the regime of PNe.

Finally, and as noted above, of the order of 97 per cent of possible PNe identifications were rejected using criteria (i)–(vi), including some 60 or so nebulae with inconsistent *IRAS* fluxes – flux ratios $S(60)/S(25)$ and $S(12)/S(25)$ which appear to place them in the regime of compact H II regions. The importance of a careful selection of sources of this type is illustrated by the recent publication of Kwok et al. (2008). Whilst this very interesting investigation is dominated by bona fide PNe, there is a doubt about whether this applies to all of the sources selected in their analysis. Certain sources (such as PNG 018.6−00.0, PNG 298.4+00.6, PNG 301.1+00.4, PNG 309.5−00.7, PNG 321.3−00.3, PNG 328.5−00.5, PNG 329.6−00.4, PNG 332.5−00.1, PNG 333.7+00.3, and PNG 340.0+00.9) appear more reminiscent of H II regions, and several (PNG 018.6−00.0, PNG 309.5−00.7, PNG 329.6−00.4, PNG 332.5−00.1) were rejected by Parker et al. (2006) on these grounds alone. *IRAS* fluxes are available for fully 70 per cent of these sources (a much higher proportion than is determined by Kwok et al.), and these appear to place the sources firmly within the regime of Galactic H II regions.

It is finally of interest to evaluate where the H II regions identified in our present study are located within the *Spitzer* colour plane, and whether these are positioned differently from the PNe, as has been suggested by Cohen et al. (2007b). Our results are shown in Fig. 1 (lower panel). It is plain from this that the distribution of H II regions does appear to differ from that of the PNe, with most of the sources occupying a very narrow range of indices [5.8] − [8.0]. However, most of the sources are also located in the box defining MASH PNe, and it is clear that there is considerable overlap between the two species of nebula – between the PNe on one hand, and compact H II regions on the other. Such *Spitzer* colours alone are therefore incapable of differentiating between these two types of object.

2.2 Criteria based on morphologies, and *IRAS* and *Spitzer* flux ratios

Preite-Martinez (1988) has used the *IRAS* Point Source Catalog to identify some 388 CPNe, where it is assumed that PNe flux ratios fall within the ranges $F(12)/F(25) \leqslant 0.35$, and $F(25)/F(60) \geqslant 0.35$. We have investigated the morphologies of those CPNe falling within the limits of the GLIMPSE MIR survey. It is clear that some of the

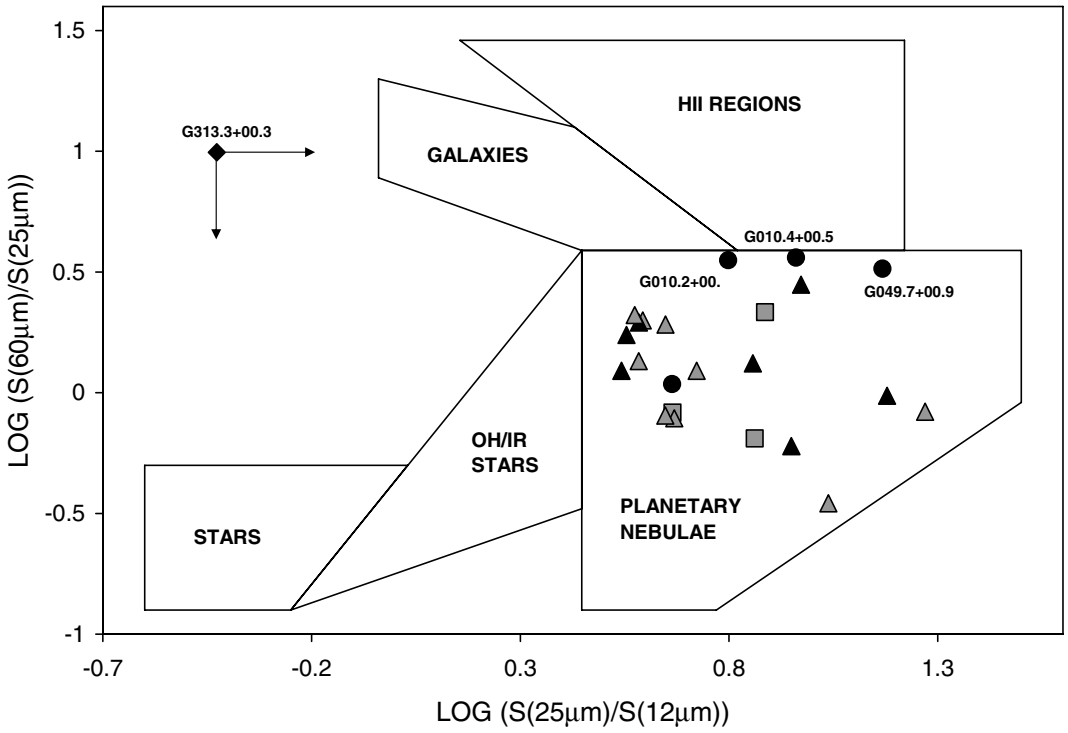

Figure 2. The location of the newly identified PNe within the *IRAS* colour plane, where the regions representing differing sources are based upon the analysis of Pottasch et al. (1988). Symbols are otherwise as indicated in Fig. 1.

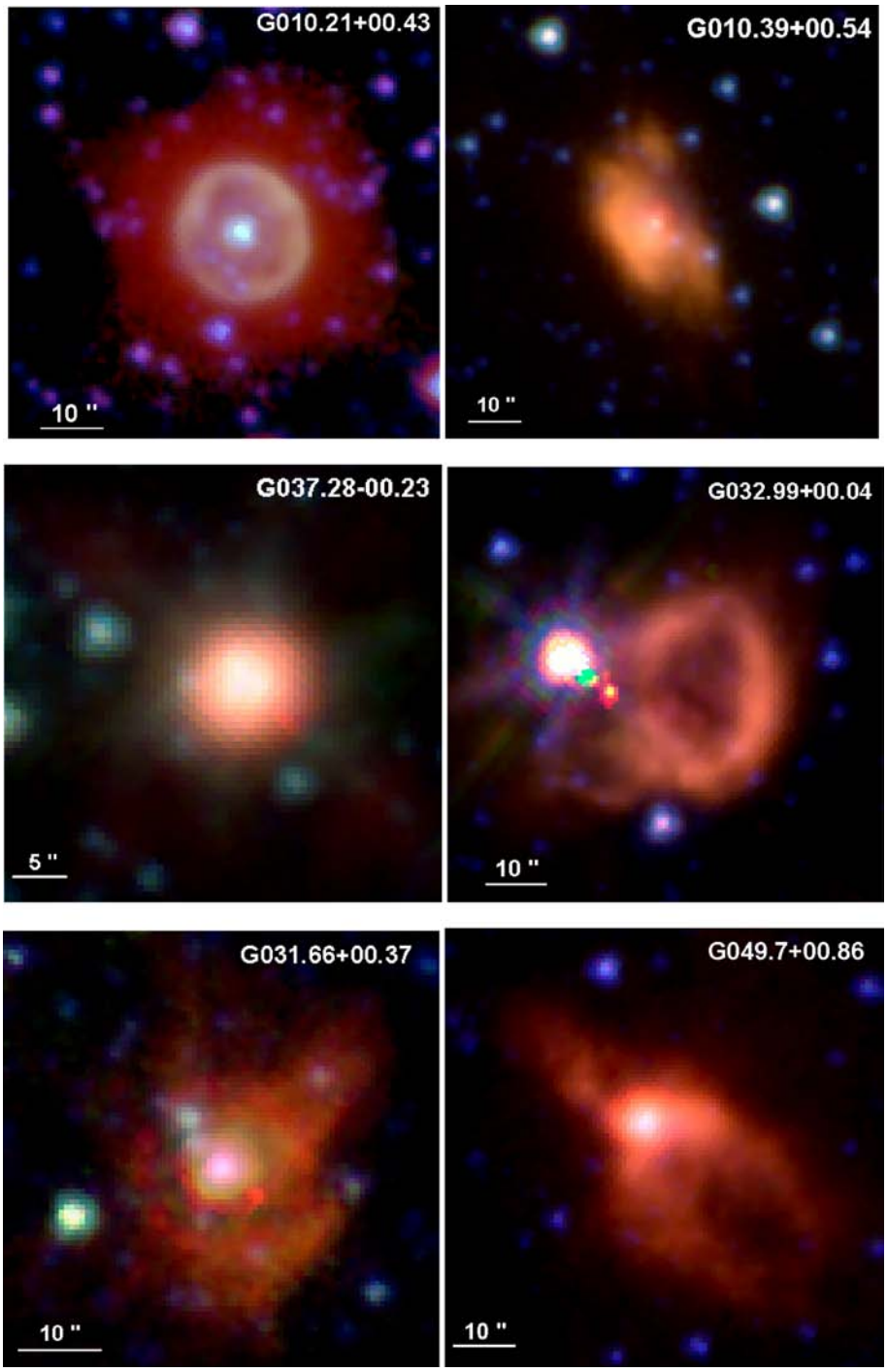

Figure 3. Colour images of six sources, where each panel represents a combination of three of our IRAC passbands. In most cases the 4.5-μm image is represented as blue, the 5.8-μm image is green, and the 8.0-μm image is red. The one exception to this is G037.28−00.23, where the 8-μm image is saturated. In this latter case, blue corresponds to 3.6 μm, green is 4.5 μm, and red corresponds to the 5.8-μm image. It will be seen that there is some tendency for the exterior (and less intense) parts of the sources to be redder than their nuclei, although this may partially result from reduced levels of extinction at longer IRAC wavelengths, increased intrinsic emission throughout the nebular shells, and the interplay of these factors with the limiting sensitivities of the maps.

sources are likely to correspond to YSOs and compact H II regions, and these have been excluded from our present analysis. Most of the other sources are spatially unresolved, or appear to be at the limits of resolution, and these have also been excluded as potential PNe (although see also our later discussion of the MIR colour plane). It is impossible, for these latter cases, to assess the true natures of the sources, or determine the likely morphologies of the emission regimes.

This leaves just seven of the sources which appear spatially resolved, details of which are provided in Table 1 (and identified as series 2 in column 6). All of these sources have what appear to be extended 'haloes', although the nuclei of the nebulae are relatively

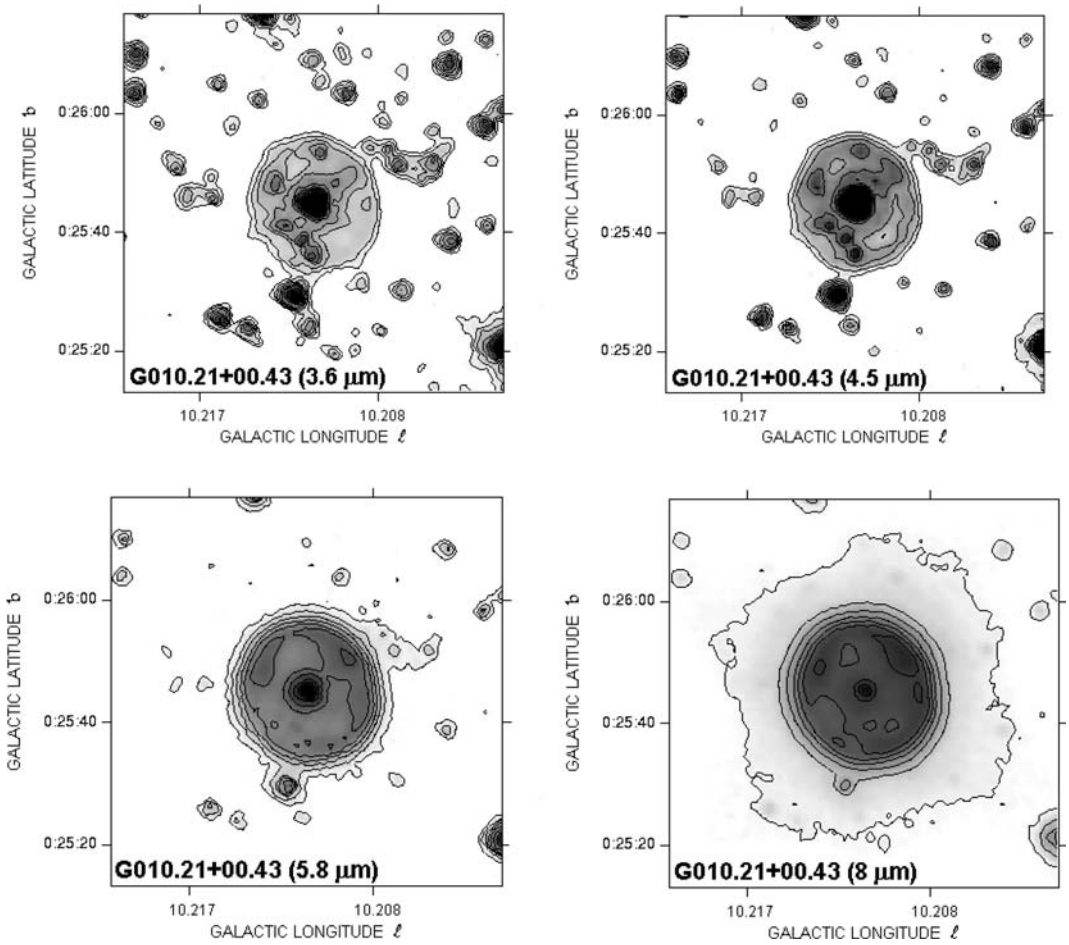

Figure 4. Contour maps for the source G010.21+00.43 in four IRAC bands. Note the presence of a bright circular interior shell, and the much fainter outer halo visible in the 8-μm map (see also the RGB image in Fig. 3). The contour parameters (A, ΔC, B, λ) are as follows: (10, 0.1888, 3.70, 3.6), (10, 0.1888, 2.62, 4.5), (25, 0.1672, 15.28, 5.8) and (55, 0.1729, 47.88, 8.0), where the parameters A, ΔC and B are as indicated in Section 2.1, and λ corresponds to the effective wavelength of the bandpass (also indicated on the lower left-hand sides of the panels).

compact. It is probable that these nuclei correspond to the primary, high emission measure ionized regimes. Contour mapping of one of the sources (G031.66+00.37) is given in Fig. 8 (later), profiles through G346.87+0.86 are provided in Fig. 15 (later), and the locations of the sources within the MIR and *IRAS* colour planes are indicated in Figs 1 and 2. In these latter cases, the resolved sources are indicated by filled triangles, whilst unresolved sources are represented by grey triangles. It is apparent that most of the Preite-Martinez sample have MIR colours similar to those of Galactic PNe, even where they appear to be unresolved, although there is perhaps a tendency for resolved nebulae to have smaller indices [5.8] − [8.0].

Very few (if any) of these sources appear to be associated with observed radio emission, suggesting that masses of ionized gas are also likely to be low – less, in all probability, than is the case for more evolved PNe. They also appear, as noted above, to have small nuclear FWHM (see Table 1). One might therefore postulate that many of the outflows are at an early stage of evolution, and have compact cores, and modest overall dimensions.

2.3 Criteria applying for 5-GHz/*IRAS* radio sources

A final set of CPNe has been identified by Becker et al. (1994), based upon the *IRAS* fluxes of compact 5-GHz sources. The authors, in this case, identify two main groups of outflow.

(i) Planetary nebulae: These are required to have $\log(F(60\,\mu\text{m})/F(25\,\mu\text{m})) \leqslant 0.6$, and $\log(F(25\,\mu\text{m})/F(12\,\mu\text{m})) \geqslant 0.6$. If the sources satisfy these constraints, and also a set of separate constraints for UC H II regions, then it is also required that $F(60\,\mu\text{m}) < 60$ Jy.

(ii) Candidate planetary nebulae: These are taken to have either $\log(F(60\,\mu\text{m})/F(25\,\mu\text{m})) \leqslant 0.6$ or the flux $F(25\,\mu\text{m})$ is an upper limit, and either $\log(F(25\,\mu\text{m})/F(12\,\mu\text{m})) \geqslant 0.5$ or the flux $F(12\,\mu\text{m})$ is an upper limit. If a source obeys the limits defining both CPNe and UC H II regions, then it is also required that $F(60\,\mu\text{m}) < 60$ Jy.

These criteria are closely similar to, but not identical with, the criteria used in Section 2.1, which are based upon the analysis provided by Pottasch et al. (1988).

Unfortunately, it appears that few (if any) of their candidate sources agree with the criteria outlined above – the majority of the sources in their table 4B appear to have been misidentified. Of the three sources which are accurately identified as potential PNe, and are located within the latitude and longitude ranges of the GLIMPSE survey, two appear to be highly compact, and of uncertain morphology. The other more extended source (G037.28 8−0.23) is illustrated in Figs 3 and 11 (later).

The positions of these sources are given in Table 1, where they are identified as Series 3 nebulae in column 6, together with

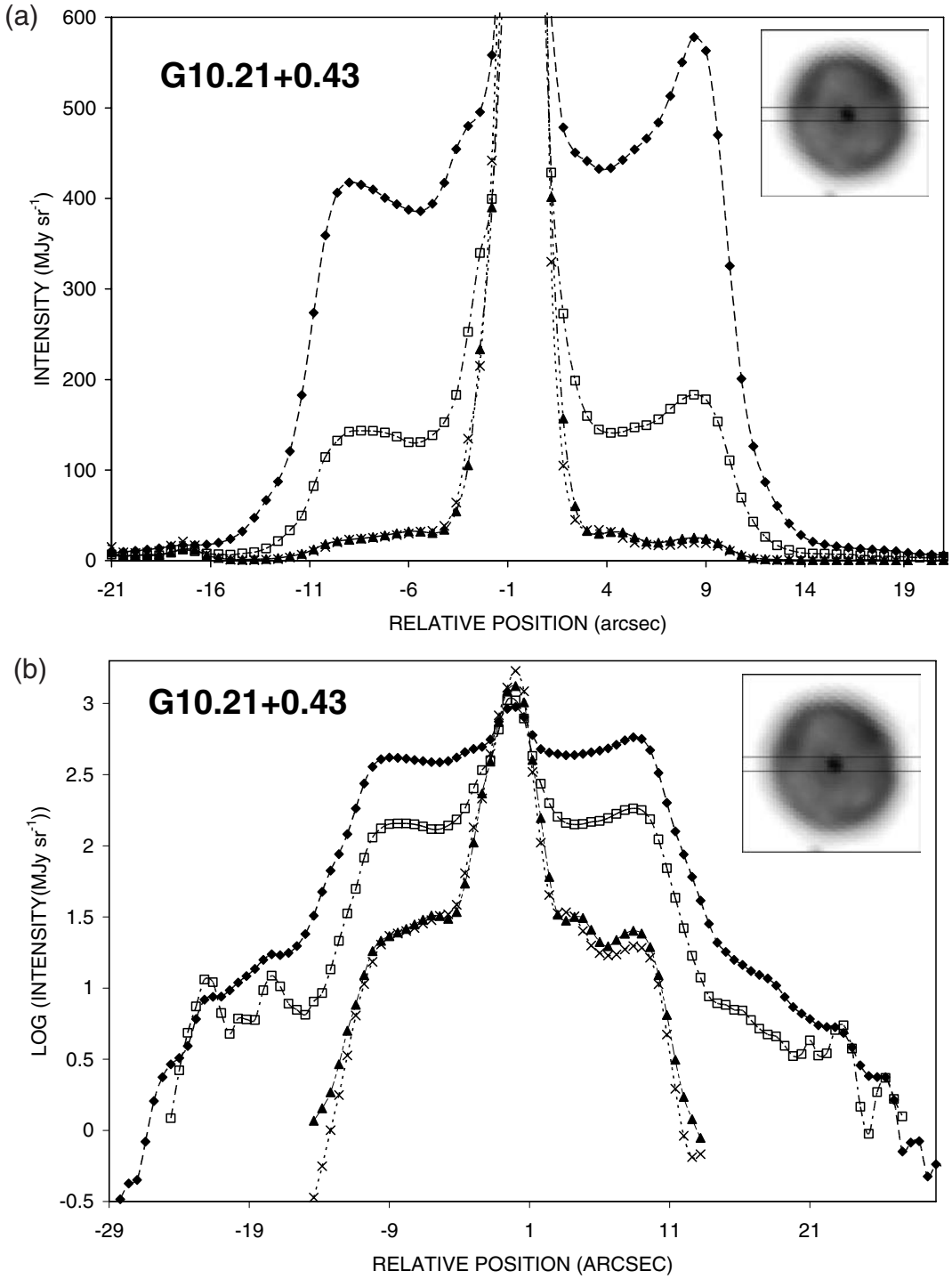

Figure 5. (a) Linear profiles through the centre of G10.21+0.43, where the positioning of the slice is indicated in the upper inset figure, and the width of the slice is 4 pixels (i.e. 2.4 arcsec). The 8-μm profile is represented by filled lozenges (and the dashed curve), whilst the 5.8-μm profile is indicated by open squares, and the dot–dashed curve. The 4.5-μm profile is defined using filled triangles and the dashed–double-dotted curve, whilst 3.6-μm trends are represented by the crosses and dotted curve. It will be noted that the 5.8- and 8.0-μm profiles, in particular, appear to show evidence for enhanced fluxes towards the edges of the primary nebular shell, and that this shell is strongly defined, and much brighter than the halo. The central peak corresponds to the central star. (b) As for (a), but with logarithmic intensity levels. These profiles show the steep decline in halo intensities out to ∼30 arcsec from the nucleus, and the sharp disparity in intensities between the nebula core and halo: the nebula appears to be ∼25 times brighter than the inner portions of the halo structure.

details of their MIR magnitudes, *IRAS* fluxes and dimensions. Profiles of G037.28 8−0.23 are illustrated in Fig. 12 (later). We have also represented the unresolved nebulae within the *Spitzer* and *IRAS* MIR colour planes (the grey squares in Figs 1 and 2). It is apparent that they have colours similar to those of Galactic PNe. The one resolved source (G037.28 8−0.23) is saturated at 8.0 μm, and this precludes an analysis within the [3.6] − [4.5]/[5.8] − [8.0] colour plane.

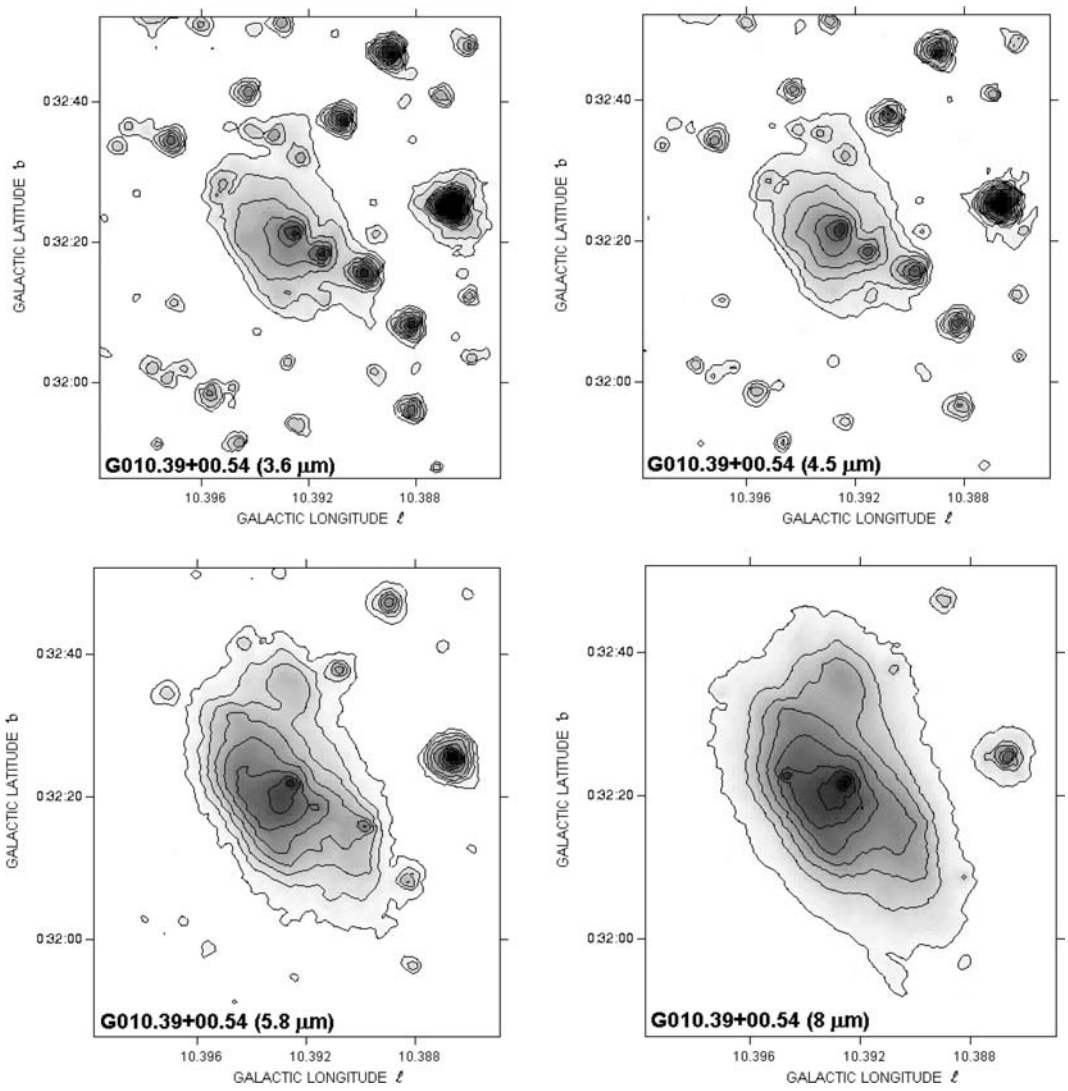

Figure 6. Contour mapping of G010.39+00.54, where the contour parameters are (10, 0.2050, 3.31, 3.6), (8, 0.2083, 2.21, 4.5), (23, 0.1713, 13.52, 5.8), (62.15, 0.1641, 50.20, 8.0). Details are otherwise as indicated in Fig. 4.

3 THE CHARACTERISTICS OF INDIVIDUAL NEBULAE

It is apparent, from the previous section, that a large fraction of the sources identified here are likely to represent high-extinction PNe. Their structures, in the case of the larger nebulae, are reminiscent of evolved Galactic PNe, although a good fraction of the nebulae also appear to be compact, and may represent younger and less evolved PN outflows. Similarly, it appears that all of the sources have *IRAS* and *Spitzer* MIR colours which are consistent with their identification as PNe.

We shall discuss the characteristics of individual sources in this present section, and undertake a more general analysis in Section 4.

3.1 G010.2+0.43

Like many other sources in this study, this nebula is identified as a PN through both its *IRAS* and *Spitzer* colours (viz. Figs 1 and 2). The envelope of the nebula has two primary components. Most of the emission arises from a nearly circular shell with diameter ∼20 arcsec [see e.g. the colour image in Fig. 3, the maps in Fig. 4, and the profiles in Figs 5(a) and (b)]. The 8-μm emission, in particular, appears to be enhanced at larger distances from the nucleus, leading to the somewhat scalloped rim structure noted in Fig. 3.

This interior shell surmounts an outer halo which appears to be particularly strong at 5.8 and 8.0 μm [see the logarithmic profiles in Fig. 5(b), and the RGB colour imaging in Fig. 3], and extends to at least ∼25 arcsec from the central star [see the RGB image in Fig. 3, and the logarithmic contours in Fig. 5(b)]. In several respects, therefore, it is apparent that the source is similar to several 'classical' PNe, and shows a particularly close resemblance to IC 418 (see e.g. the discussion of near-IR (NIR) imaging of this source, and of its hot dust halo in Phillips & Ramos-Larios 2005). The fact that outer halo fluxes are strong at longer wavelengths may be interpreted in a variety of ways, including continuum emission by small (photon-heated) grains (see e.g. Phillips et al. 1984; Borkowski et al. 1994; Phillips & Ramos-Larios 2005, 2006, 2007), and/or polycyclic aromatic hydrocarbon (PAH) emission bands. In either case, it is likely that the emitting agents are located in an outer photodissociative regime (PDR) (see the further discussion in Section 4).

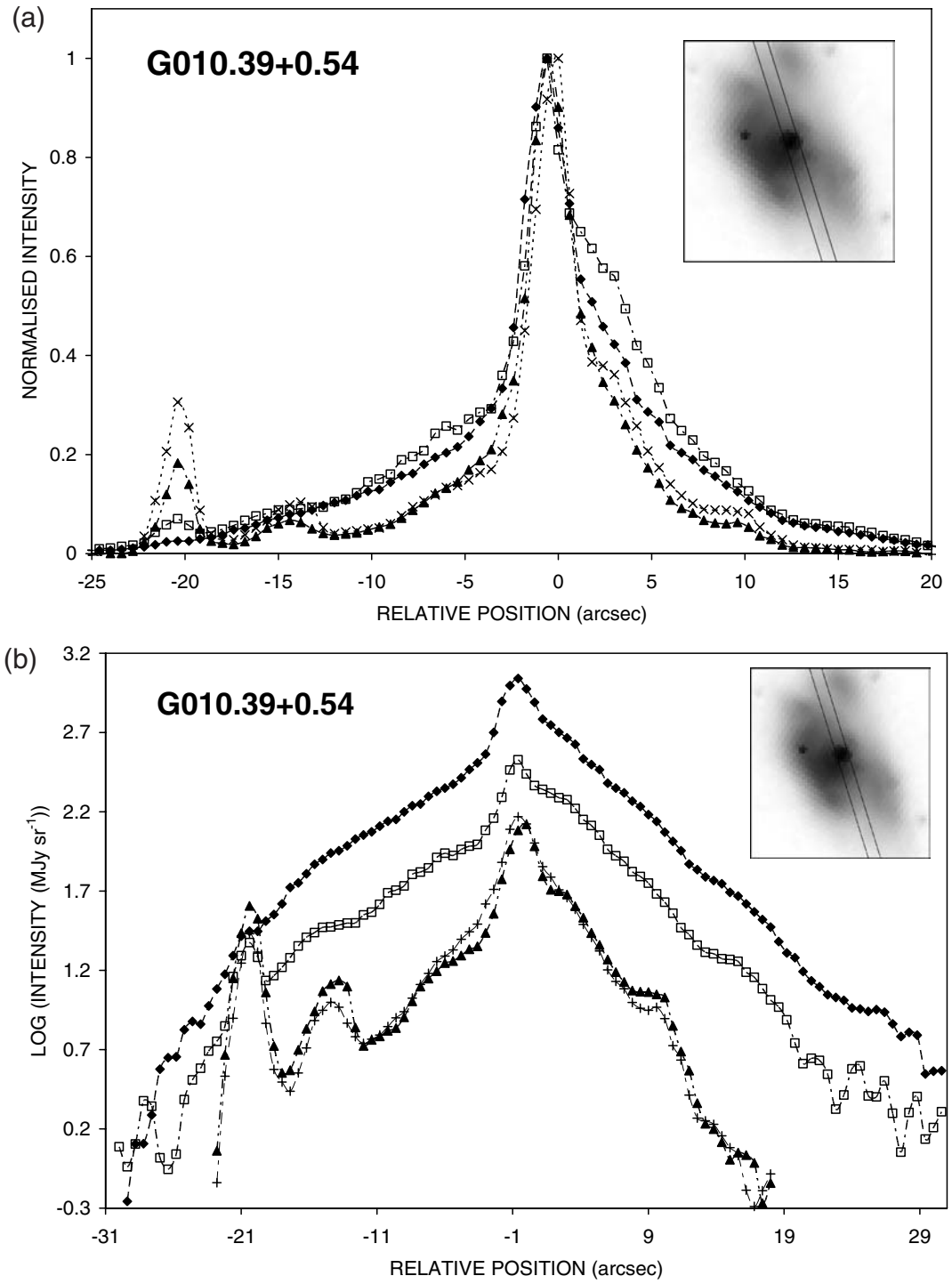

Figure 7. (a) Normalized profiles through the source G010.39+0.84, where it will be seen that emission falls off extremely steeply away from the nucleus. The width of the profile is 2.4 arcsec, and details are otherwise as indicated in Fig. 5(a). (b) As for (a), but for logarithmic intensities in units of MJy sr^{-1}. These show, far more clearly than was possible in (a), the regular fall-off in intensities outside of the nucleus. Details are otherwise as indicated in Fig. 5(a).

Finally, the presence of a bright and well-defined central star makes it possible to obtain rough estimates for the foreground interstellar extinction. We find that the central star has indices [3.6] − [4.5] $\cong$ 0.33 $\pm$ 0.01 mag and [5.8] − [8.0] $\cong -0.21^{+0.42}_{-0.60}$ mag, where much of the uncertainty is attributed to background and nebular subtraction. If one assumes that the intrinsic indices of the stars are closer to 0.0 (see e.g. the stellar IRAC band modelling of Whitney et al. 2003, and the IRAC calibration of Reach et al. 2005), and one takes the IRAC extinction coefficients of Indebetouw et al. (2005), and a value A_K/A_V appropriate for $R_V = 3.1$ (Cardelli, Clayton & Mathis 1989), then this implies that levels of A_V must be of the order of $\approx$23.6 mag.

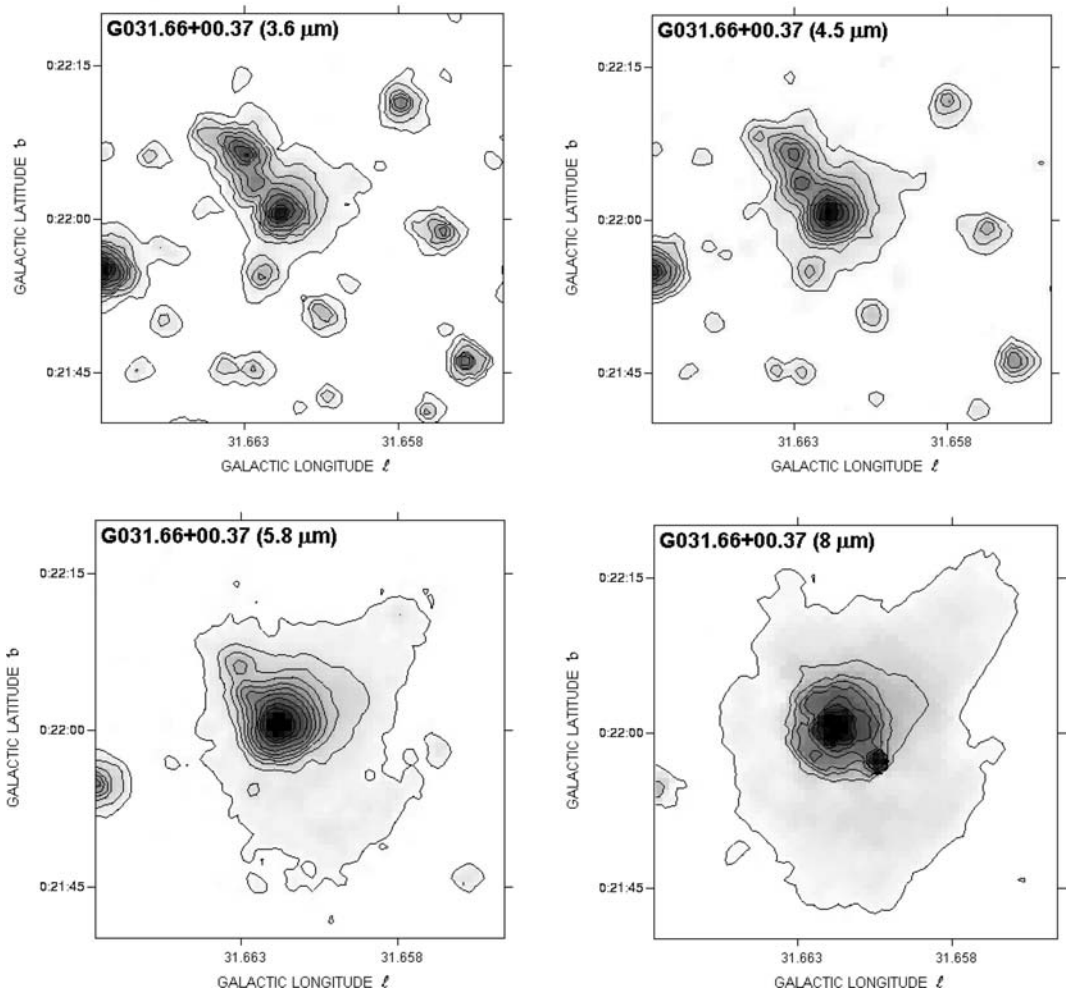

Figure 8. Contour mapping for G031.66+00.37, where contour levels are given by (7, 0.1952, 4.00, 3.6), (6, 0.2222, 2.33, 4.5), (33, 0.1312, 24.67, 5.8) and (65, 0.1603, 80.61, 8.0). Note the evidence for extended emission in the longer wave channels. Details are otherwise as indicated in Fig. 4.

3.2 G010.39+0.55

This source shows evidence for a somewhat diffuse ellipsoidal shell, with a possible exciting star located west of the nebular centre (Figs 3 and 6). There also appears to be evidence for a north-west condensation located some 16 arcsec from the centre. Logarithmic and linear profiles along the major axis of the source, and through the putative central star, show the presence of a highly compact nuclear regime; a zone which is barely resolved at shorter wavelengths, but has a deconvolved FWHM of ∼3.7 arcsec at 8 μm, and ∼5.3 arcsec at 5.8 μm (Figs 7a and b). Emission outside of this regime falls off rapidly with increasing radius, and appears to vary in a manner similar to that observed in NGC 6302 and 6537 (see Phillips & Ramos-Larios 2008). It also extends over a region with size >56 arcsec. It is therefore possible that the source is a further example of a bipolar outflow, albeit with a structure which is far from being well defined.

3.3 G031.66+0.37

This nebula is one of Preite-Martinez group of objects, and appears to be firmly ensconced within the PNe regime of the *IRAS* colour plane – there appears to be little likelihood that it could be an H II region, for instance. The source is illustrated through contour mapping in Fig. 8, and in the RGB imaging in Fig. 3. In this case, the nuclear region of the source is hardly (if at all) resolved, and surrounded by a halo which appears to be weak, spheroidal and somewhat irregular. The RGB images also show that the halo is much redder than the nucleus (i.e. particularly strong at longer wavelengths), and afflicted by a range of instrumental contaminants, including the diffraction pattern of the central source. It is conceivable that this outer halo is tracing the nebular PDR.

3.4 G032.99+0.04

This source has a classical elliptical shell comparable to that of many other PNe, although with some evidence for disruption (or extension) towards the north-east (i.e. the lower left-hand side of Figs 3 and 9). The *IRAS* and MIR fluxes of this nebula place it firmly within the PNe colour regime (Figs 2 and 3). Normalized profiles through the source show strong peak/centre flux ratios, and similar trends in all four IRAC bands, although it seems that the left-hand peak (at relative position RP = −14 arcsec) becomes relatively weaker at 5.8 and 8.0 μm (Fig. 10).

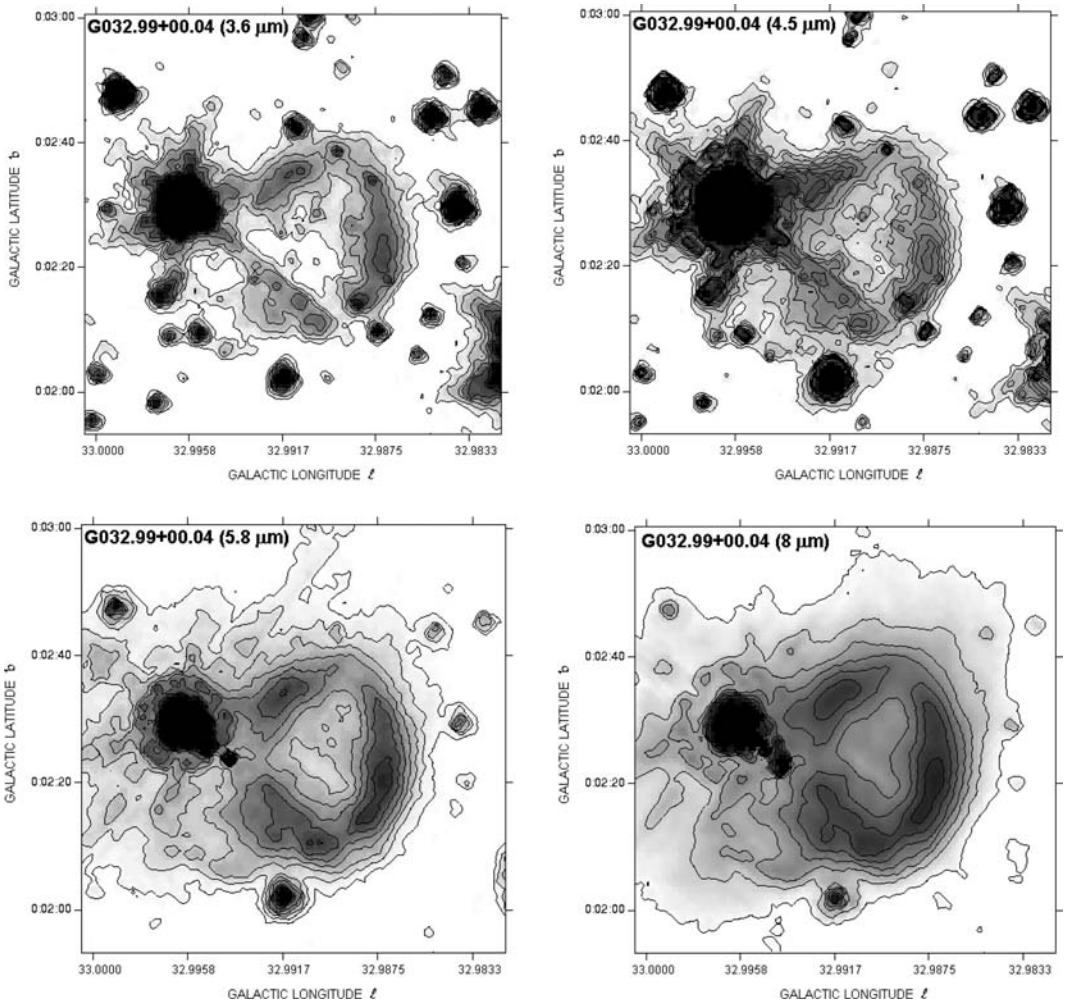

Figure 9. Contour mapping for G032.99+00.04, where contour levels are given through (8, 0.1219, 3.54, 3.6), (7, 0.0777, 2.55, 4.5), (36, 0.1270, 22.56, 5.8) and (80.02, 0.1250, 67.0, 8.0). The dark spot to the left-hand side of centre corresponds to a bright field star, together with associated diffraction spikes. Details are otherwise as indicated in Fig. 4.

3.5 G037.28−00.23

This represents the one clear, resolved PN detected using the 5-GHz/*IRAS* search criteria of Becker et al. (1994), and we have illustrated contour maps in Fig. 11, an RGB colour image in Fig. 3, and profiles in Fig. 12. The 8-μm imaging and profiles are saturated, and have not been included in this analysis.

It is clear from these that the source is reasonably well resolved and circular, with some nuclear peaking at shorter wavelengths which may be indicative of central star emission.

3.6 G049.70+0.86

This source appears to have a bipolar structure and bright (barely resolved) core. It is clear that the bipolar structure is very much stronger at longer wavelengths, a characteristic which is apparent though contour mapping (Fig. 13), the RGB image (Figs 3), and logarithmic profiles through the centre of the source (Fig. 14). Emission falls off steeply outside of the central nucleus, by a factor of ∼15 or so between RP = 5 and 28 arcsec (and RP = −5 and −18 arcsec), and a further factor of 20 or so between RP = −18 and −20 arcsec; it would therefore seem that there are reasonably well-defined limits close to RP ≅ −18 arcsec, and RP ≅ 28 arcsec. This fall-off in intensity is reminiscent, yet again, of that observed in other bipolar PNe (Phillips & Ramos-Larios 2008).

3.7 G0346.68+0.86

This is representative of other sources in Table 1 which, whilst having nuclei that are clearly resolved and spherical, are nevertheless extremely compact, and at the limits of what this present analysis can achieve. Profiles through the nucleus of the source are illustrated in Fig. 15, and appear to show comparable trends at all but the shortest wavelength.

4 DISCUSSION

It appears likely, from the analysis above, that the GLIMPSE survey has been useful in identifying several new and high-extinction PNe. We have employed two primary procedures in our search for these nebulae. In the first place, we have investigated the extant GLIMPSE data base for morphologically promising emission structures, and filtered out those of the sources with appropriate MIR/FIR colours. We have also checked the morphologies of sources which have been identified as CPNe on the basis of prior analyses of the *IRAS* Catalog.

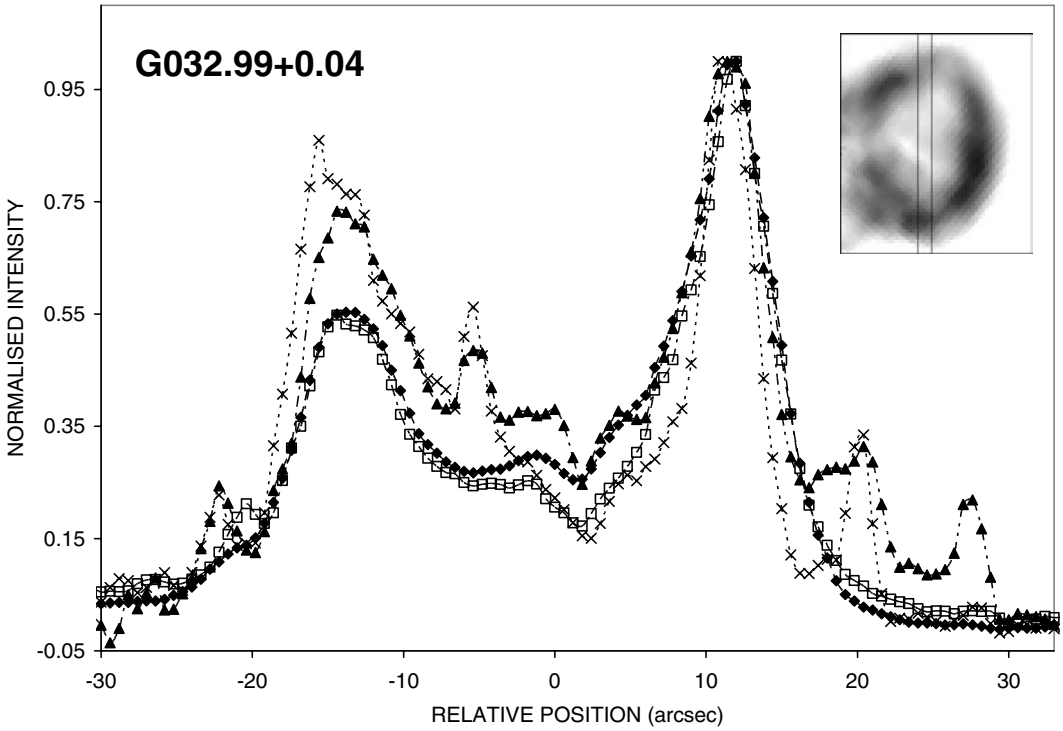

Figure 10. Profiles through the centre of G032.99+0.04, showing a marked double-peaked structure associated with the ring morphology. The width of the profile is 2.4 arcsec, and details are otherwise as indicated in Fig. 5(a).

The resulting list of newly identified PNe is presented in Table 1.

Analysis and mapping of these sources show that there is a tendency for emission to be more extended at longer wavelengths (5.8 and 8 μm) than at shorter wavelengths; a trend which has previously been noted in other PNe as well (Phillips & Ramos-Larios 2008). Several of the sources also have haloes which appear to be particularly enhanced at longer wavelengths. Some of this longer wave enhancement may be due to decreased levels of longer wave extinction, together with an increase in emission throughout the nebular shells. This means that whilst weaker emission features and haloes are readily apparent in the longer wave channels, they sink below levels of detectability in the 3.6- and 4.5-μm bands. If this is the case, then it may give an impression of false colour gradients, such that nuclei appear bluer than is the case for outerlying structures.

However, it should be noted that since the differential extinction at these wavelengths is extremely small (Indebetouw et al. 2005), the influence of variable extinction can only be of importance where values of A_v are very large – say of the order of >50 mag or so, which would lead to values $A_{3.6\,\mu m} - A_{4.5\,\mu m} > 0.7$ mag. Similarly, and even in this case, it is not entirely clear that there is *any* significant difference in extinction between 4.5 and 8 μm – and where there is, it may even be possible that it operates in a reverse way to that observed at shorter wavelengths, such that extinctions at 8 μm are greater than in the intermediate IRAC passbands. Thus for instance, various models suggest that there may be strong ISM silicate absorption at $\lambda \sim 10\,\mu m$, extending down as far as the 8-μm photometric band (see e.g. Cohen 1993, and the reddening vectors of Whitney et al. 2003). This, if true, would lead a reduction in the indices [5.8] − [8.0].

So the role of extinction is far from clear, but is probably not unduly critical in the interpretation of these results. On the other hand, there is plenty of evidence to show that emission may increase between the shorter and longer wave passbands [see e.g. the *ISO* spectra illustrated by Hora et al. (2004) and Phillips & Ramos-Larios (2008)]. Indeed, it would appear difficult to explain many of the present trends unless there is some such variation in fluxes. Given that this is the case, however, it is apparent that the extended halo-type structures are unlikely to arise due to 'normal' grain emission processes – through, say, the direct stellar irradiation of ∼0.1-μm grains (see e.g. the discussion in Phillips & Ramos-Larios 2008). Given normal central star luminosities and temperatures, for instance, then it is apparent that levels of heating flux would be much too small. It has therefore been argued that such emission may arise due to very small grains of the order of ⩽100 Å in size, in which the absorption of photons leads to large (and secularly short) excursions in temperature (see e.g. Draine 2003). Evidence for the presence of such grains outside of the primary ionized regimes has been presented by Borkowski et al. (1994), Phillips et al. (1984) and Phillips & Ramos-Larios (2005, 2006, 2007), where it has been argued that they lead to continuum excesses in the NIR. In addition, the 5.8- and 8-μm IRAC bands contain PAH features at 6.2, 7.7 and 8.6 μm, due to a combination of C–C stretching and C–H in plane bending modes (see e.g. Tielens 2005), and it is conceivable that fluorescent excitation of the bands may be responsible for the observed (and enhanced) longer wave emission. Spectral evidence for such bands has been provided by various authors (see e.g. Bernard-Salas et al. 2001, 2006; Cernicharo et al. 2001; Molster et al. 2002; Volk & Kwok 2003; Hora et al. 2004; Bernard-Salas 2006; Kraemer et al. 2006; Phillips & Ramos-Larios 2008). In addition, it is apparent that the PAH emission bands are often associated with pseudo-continua, whose origin is a matter of continuing uncertainty. These may, in certain cases, represent inherently broader structures, and in others consist of narrower (but closely spaced, and spectrally unresolved) features. Similarly, it has been noted that such features may arise

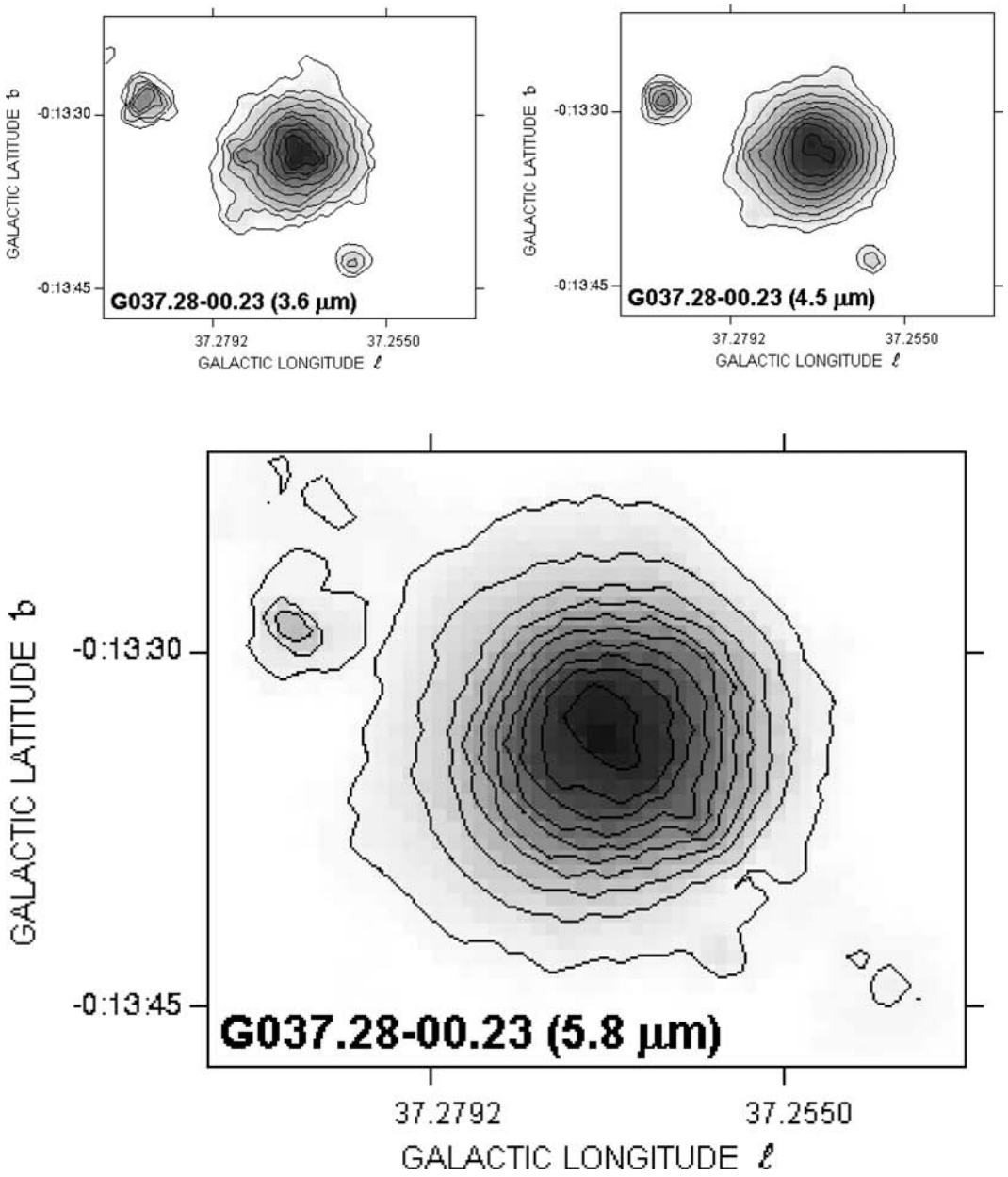

Figure 11. Contour mapping for G037.28−00.23, where it should be noted that the 8.0-μm map is saturated, and has not been included here. The contour levels are given through (25, 0.2310, 3.94, 3.6), (30, 0.2222, 3.00, 4.5) and (65, 0.2096, 34.21, 5.8), and details are otherwise as noted in Fig. 4. The circularity of the envelope is also apparent in Fig. 3.

from combinations of 350–600 C atoms, not formed into single planar PAH species, but rather into three-dimensional clusters of smaller PAH grains, held together by either van der Waals bonds or aliphatic chains.

In any case, and whatever their origins may be, it is clear that such continua may contribute an appreciable fraction to the overall PAH emission budget.

Where such emission arises due to very small grains, and/or due to the PAH-type molecules hosted by these grains, it is likely that their lifetimes will be dependent upon both the environment in which they reside, and the sizes of the grains. Densities which are too high, and temperatures which are too great would lead to a strong reduction in the lifetimes of both of these agents, depending upon the sizes of the grains concerned. Similarly, grains less than 50 atoms in size may have difficulty in surviving over the lifetime of the PNe, although larger ones may prove to be much more durable, as has been noted by Allain, Leach & Sedlmayr (1996a,b).

It is therefore likely that much of the longer wave emission, particularly that arising in haloes, may arise in lower density (and temperature) PDRs. It is also possible that shocks at the limits of the ionized shells, associated perhaps with the outer ionization fronts, may be leading to the break up of larger grains, and the replenishment of smaller grains and/or PAH molecular carriers (e.g. Jones, Tielens & Hollenbach 1996).

We have, so far in this discussion, concentrated upon possible grain and molecular contributions to the observed nebular

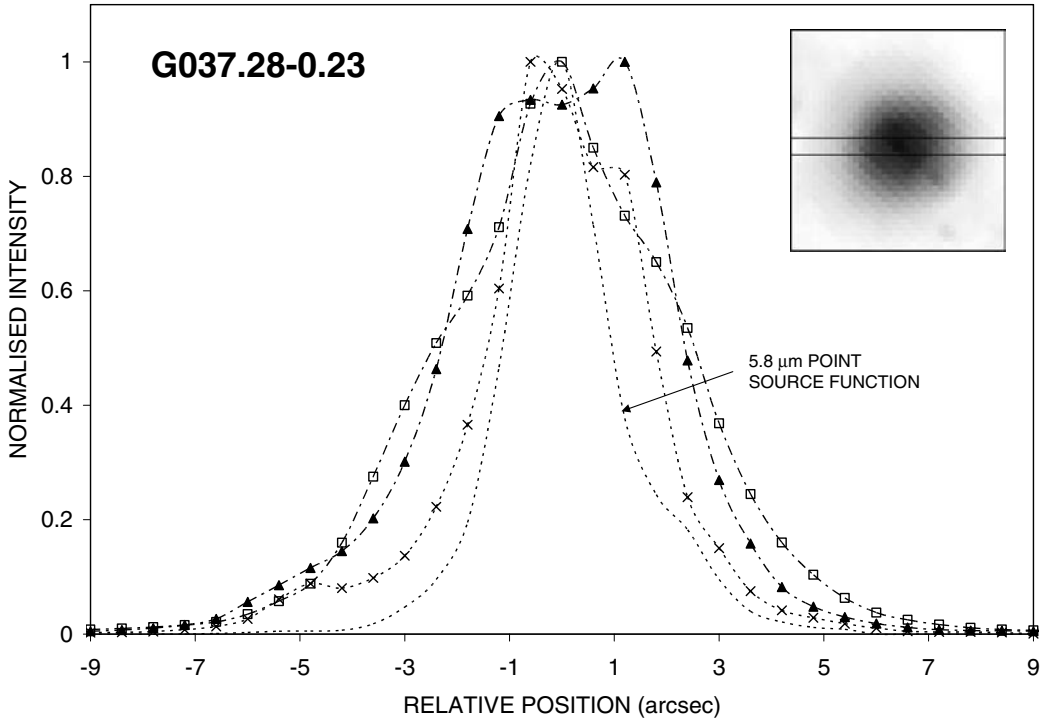

Figure 12. Normalized profiles through G037.28−0.23, where it will be noted that the trends are markedly different in the three IRAC passbands. Whilst the source is certainly compact, it is also reasonably well resolved. The width of the profile is 1.8 arcsec, and details are otherwise as indicated in Fig. 5(a).

structures. This short-changes the possible contribution due to molecular hydrogen, however, which has been shown to be important at both near and MIR wavelengths. Thus for instance, NIR H_2 transitions have been observed for a broad range of such nebulae (see e.g. Storey 1984; Greenhouse, Hayward & Thronson 1988; Kastner et al. 1994; Latter et al. 1995; Allen et al. 1997; Ramos-Larios & Phillips 2006), where they are usually assumed to be excited by shocks (see e.g. Draine, Roberge & Dalgarno 1983; Hollenbach & McKee 1989), UV pumping (e.g. Black & Dalgarno 1976; Black & van Dishoeck 1987; Sternberg & Dalgarno 1989; Burton, Hollenbach & Tielens 1990a,b; Natta & Hollenbach 1998) and/or soft X-ray emission (Phillips 2006b). There is also evidence that this emission is located outside of the primary ionized regimes (see e.g. Beckwith, Persson & Gatley 1978; Graham et al. 1993; Hora & Latter 1994; Guerrero et al. 2000; Ramos-Larios & Phillips 2006), suggesting an origin in the nebular PDRs. It therefore comes as no surprise to find that such emission may be strong at MIR wavelengths as well, and has been observed and mapped within NGC 7293 (Hora et al. 2006).

At least some of the extended emission may therefore derive from shock or fluorescently excited H_2. By contrast, whilst low excitation forbidden atomic lines also emit in the PDRs, these are particularly strong between 35 and 158 μm, and therefore lie outside of the presently observed IRAC photometric regime (see e.g. Bernard-Salas & Tielens 2005). If the more extended halo-type formations are due to forbidden line transitions, then it is possible that we are dealing with higher excitation species (such as [Ar III] and [Ne VI]), and observing fully ionized structures.

Finally, it is well established that grains within the ionized regimes would be prone to absorbing resonantly trapped Lyα photons, and this thermostatically constrains the temperatures of the particles to lie somewhere near 120 K (see e.g. Cohen & Barlow 1974). Such temperatures drive the bulk of emission to wavelengths of ∼25 μm or longer, however, outside of the range covered by the present IRAC photometric bands.

Whatever the primary emission mechanism might be, whether it involves PAH features, warm dust continua, shock or fluorescently excited H_2 lines, or forbidden lines, it is apparent that the present nebular structures are reminiscent of those for other, and better known PNe, and confirm the emission trends noted by Hora et al. (2004), Phillips & Ramos-Larios (2008), Bernard-Salas et al. (2006), Cohen et al. (2005) and Kraemer et al. (2006). It is to be hoped that further extension of the GLIMPSE or other large-scale *Spitzer* programmes may allow further advances to be made in the detection of new PNe. It is also probable that many much fainter PNe structures are still waiting to be discovered, and would become evident through an even longer (and more painstaking) survey of the present GLIMPSE data base. Finally, we note that ∼2/3 of the brighter, and more extended MASH and Acker et al. nebulae were 'rediscovered' in this analysis, including the source G313.3+00.3 of Cohen et al. (2005). The fact that at least a third of known nebulae were not picked up therefore suggests that many brighter sources remain to be detected. This applies, in particular, at very low Galactic latitudes, where such nebulae are difficult to distinguish from the panoply of other emission structures.

5 CONCLUSIONS

We have undertaken a search for new (and high-extinction) PNe close to the Galactic plane, using data products associated with the *Spitzer* GLIMPSE survey. This has involved searching for nebulae having appropriate morphologies within the ranges $|b| \leqslant 1^\circ$, and $|l| = 10^\circ$–65°, and also having MIR and *IRAS* colours typical of Galactic PNe. We have also investigated sources which have previously been identified as CPNe on the basis of their colours within the *IRAS* Point Source Catalog.

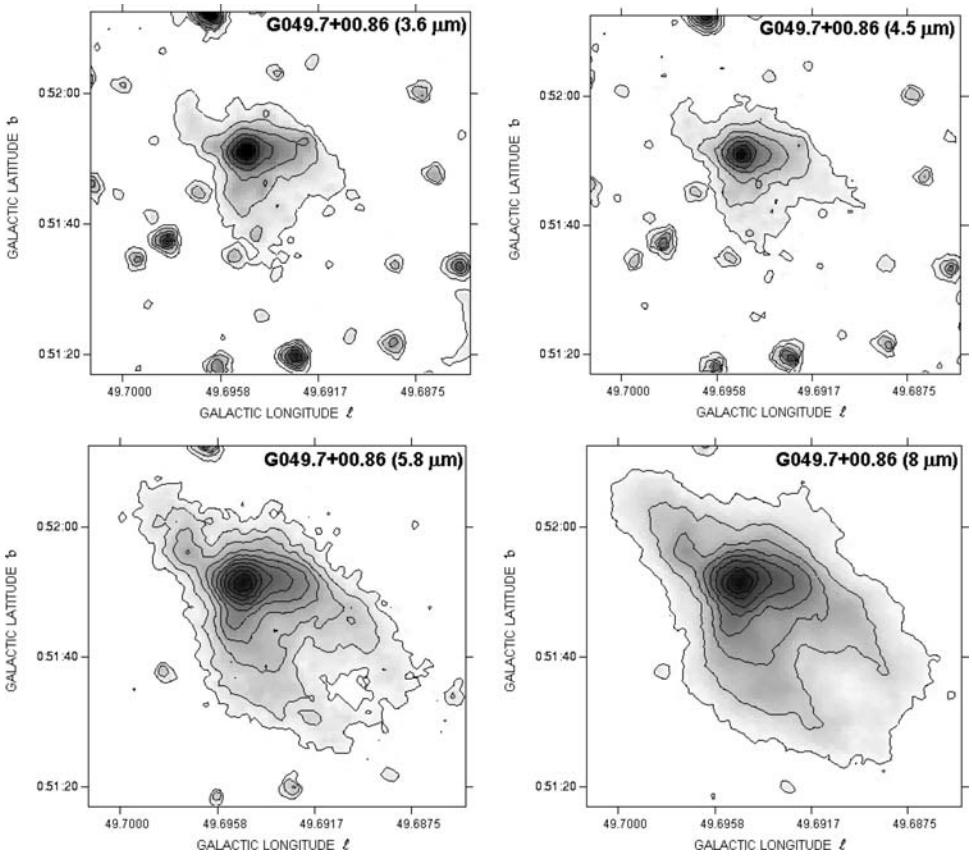

Figure 13. Contour mapping for the source G049.70+00.86, where the contour levels are given through (3.5, 0.2621, 1.27, 3.6), (2.5, 0.2840, 0.78, 4.5), (10, 0.1780, 4.67, 5.8) and (23, 0.1908, 14.56, 8.0). Details are otherwise as indicated in Fig. 4.

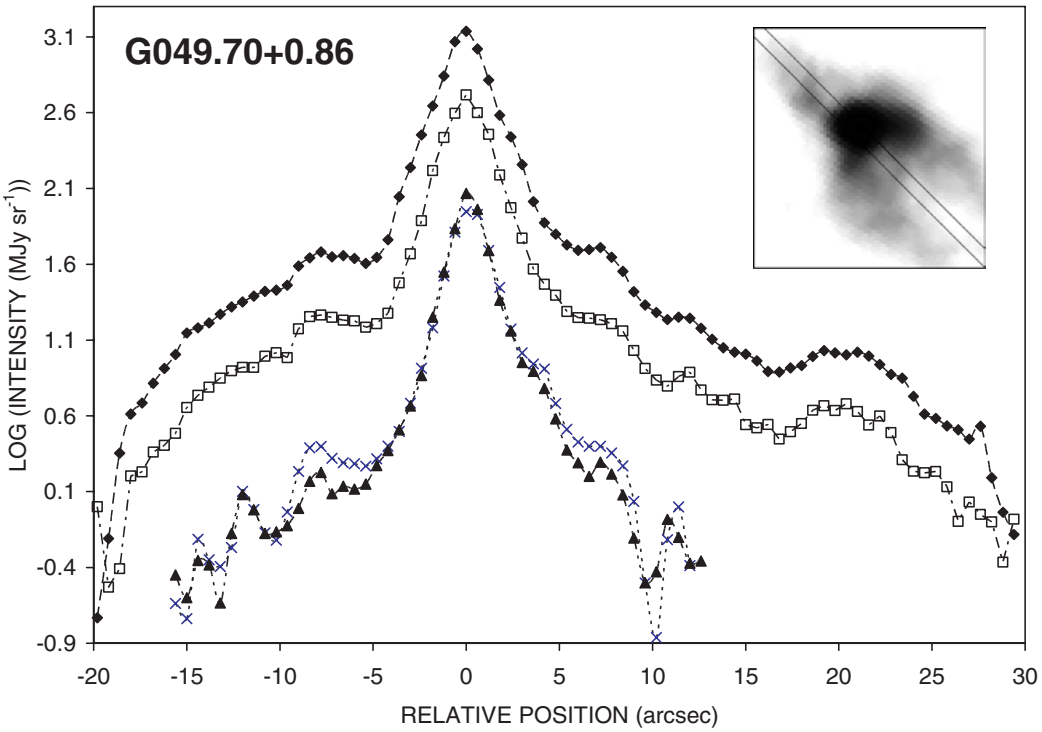

Figure 14. Logarithmic profiles through G049.70+00.86, where it is apparent that intensities fall-off very steeply outside the core. The width of the profile is 2.4 arcsec, and details are otherwise as indicated in Fig. 5(a).

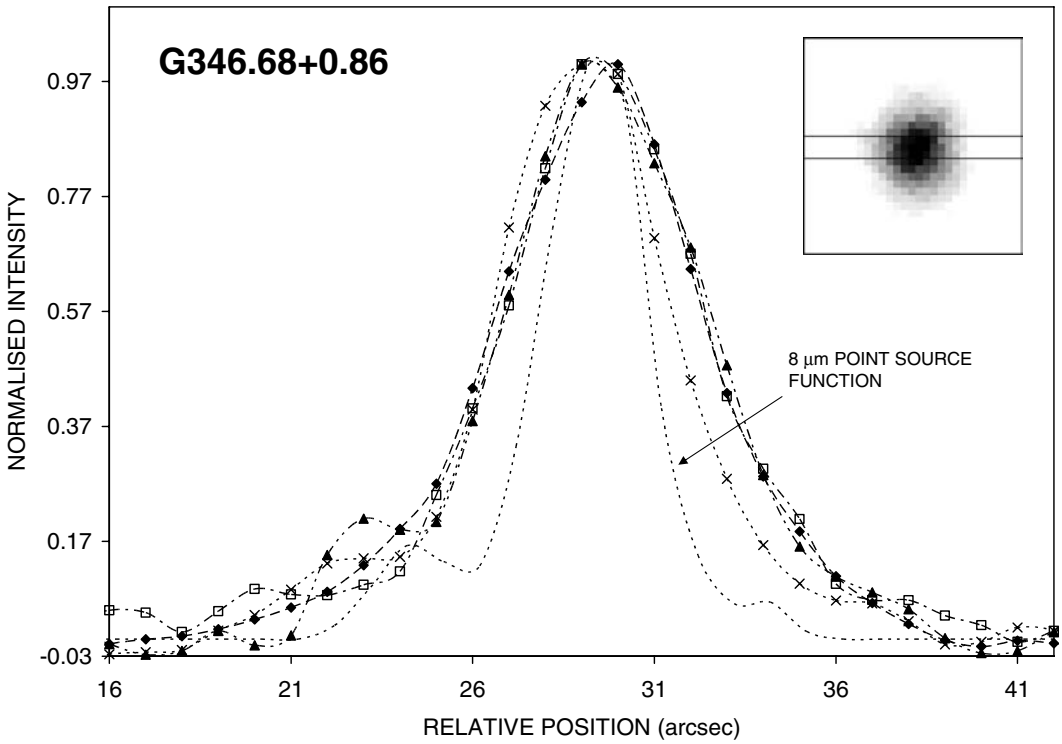

Figure 15. Normalized profiles through the highly compact source G346.68+0.86. This source is typical of several of the compact nebulae listed in Table 1. The width of the profile is 1.8 arcsec, and details are otherwise as indicated in Fig. 5(a).

This time-consuming project yielded a modest total of 12 probable PNe. We also noted that many unresolved sources have colours similar to those of PNe, although it was impossible to further verify their status using morphological criteria.

We have undertaken calibrated contour mapping of the larger fraction of these sources, as well as taking profiles through their shells, and superimposed RGB colour imaging of the envelopes, in an attempt to further clarify the nature of the shells, and determine how their morphologies vary with wavelength. We note that the sources are typically broader at longer wavelengths (5.8 and 8.0 μm) than is the case at 3.6 and 4.5 μm, and appear to be characterized by high surface brightness nuclei, and very much weaker halo-type structures. The 'halo' regimes are particularly evident at longer IRAC wavelengths, where it is possible that emission is dominated by small grain continua and/or PAH emission bands. It is suggested that many of these envelopes may represent PDRs, and appear characteristic of what is observed in other PNe.

Although it has been proposed that the proportion of bipolar nebulae should increase towards lower Galactic latitudes (their angular scale heights are smaller than for other categories of source; see e.g. Phillips 2001), we have noted only two possible examples of such sources within the present data trawl.

ACKNOWLEDGMENTS

This work is based, in part, on observations made with the *Spitzer Space Telescope*, which is operated by the Jet Propulsion Laboratory, California Institute of Technology, under a contract with NASA. Support for this work was provided by an award issued by JPL/Caltech. GR-L also acknowledges the support of a postgraduate scholarship from CONACyT (Mexico).

REFERENCES

Allain T., Leach S., Sedlmayr E., 1996a, A&A, 305, 602
Allain T., Leach S., Sedlmayr E., 1996b, A&A, 305, 616
Allen L. E., Ashley M. C. B., Ryder S. D., Storey J. W. V., Sun Y.-S., Burton M. G., 1997, in Habing H. J., Lamers H. J. G. L. M., eds, Proc. IAU Symp. 180, Planetary Nebulae. Kluwer, Dordrecht, p. 205
Aumann H. H., Fowler J. W., Melnyk M., 1990, AJ, 99, 1674
Becker R. H., White R. L., Helfand D. J., Zoonematkermani S., 1994, ApJS, 91, 347
Beckwith S., Persson S. E., Gatley I., 1978, ApJ, 219, L33
Benjamin R. A. et al., 2003, PASP, 115, 953
Bernard-Salas J., 2006, in Barlow M. J., Mendez R. H., eds, Proc. IAU Symp. 234, Planetary Nebulae in our Galaxy and Beyond. Cambridge Univ. Press, Cambridge, p. 181
Bernard-Salas J., Pottasch S. R., Beintema D. A., Wesselius P. R., 2001, A&A, 367, 949
Bernard-Salas J., Tielens A. G. G. M., 2005, A&A, 431, 523
Bernard-Salas J., Peeters E., Sloan G. C., Cami J., Guiles S., Houck J. R., 2006, ApJ, 652, 29
Black J. H., Dalgarno A., 1976, ApJ, 203, 132
Black J. H., van Dishoeck E. F., 1987, ApJ, 322, 412
Borkowski K. J., Harrington J. P., Blair W., Bregman J. D., 1994, ApJ, 435, 722
Burton M. G., Hollenbach D. J., Tielens A. G. G. M., 1990a, ApJ, 365, 620
Burton M. G., Hollenbach D. J., Tielens A. G. G. M., 1990b, ApJ, 399, 563
Cahn J. H., Kaler J. B., 1971, ApJS, 22, 319
Cardelli J. A., Clayton G. C., Mathis J. S., 1989, ApJ, 345, 245
Cernicharo J., Heras A. M., Tielens A. G. G. M., Pardo J. R., Herpín F., Guelin M., Waters L. B. F. M., 2001, ApJ, 546, 123
Cohen M. J., 1993, AJ, 105, 1860
Cohen M., Barlow M. J., 1974, ApJ, 193, 401
Cohen M. et al., 2005, ApJ, 627, 446
Cohen M. et al., 2007a, MNRAS, 374, 979
Cohen M. et al., 2007b, ApJ, 669, 343

Draine B. T., 2003, ARA&A, 41, 241
Draine B. T., Roberge W. G., Dalgarno A., 1983, ApJ, 264, 485
Fazio G. et al., 2004, ApJS, 154, 10
Garcia-Lario P., Manchado A., Pottasch S. R., Suso J., Olling R., 1990, A&AS, 82, 497
Garcia-Lario P., Manchado A., Pych W., Pottasch S. R., 1997, A&AS, 126, 479
Graham J. R., Herbst T. M., Matthews K., Neugebauer G., Soifer B. T., Serabyn E., Beckwith S. 1993, ApJ, 408, L105
Greenhouse M. A., Hayward T. L., Thronson H. A., 1988, ApJ, 325, 604
Guerrero M. A., Villaver E., Manchado A., Garcia-Lario P., Prada F., 2000, ApJS, 127, 125
Hora J. L., Latter W. B., 1994, ApJ, 437, 281
Hora J. L., Latter W. B., Allen L. E., Marengo M., Deutsch L. K., Pipher J. L., 2004, ApJS, 154, 296
Hora J. L., Latter W. B., Smith H. A., Marengo M., 2006, ApJ, 652, 426
Hora J. L. et al., 2008, AJ, 135, 726
Hollenbach D., McKee C. F., 1989, ApJ, 342, 306
Indebetouw R. et al., 2005, ApJ, 619, 931
Jones A. P., Tielens A. G. G. M., Hollenbach D. J., 1996, ApJ, 469, 740
Kastner J. H., Gatley I., Merrill K. M., Probst R., Weintraub D. A. 1994, ApJ, 421, 600
Kraemer K. E., Sloane G. C., Bernard-Salas J., Price S. D., Egan M. P., Wood P. R., 2006, ApJ, 625, 25
Kwok S., 2000, The Origin & Evolution of Planetary Nebulae. Cambridge Univ. Press, Cambridge
Kwok S., Zhang Y., Koning N., Churchwell E., 2008, ApJS, 174, 426
Latter W. B., Kelly D. M., Hora J. L., Deutsch L. K. 1995, ApJS, 100, 159
Leene A., Pottasch S. R., 1987, A&A, 173, 145
Manchado A., Pottasch S. R., Garcia-Lario P., Esteban C., Mampaso A., 1989, A&A, 214, 139
Molster F. J., Waters L. B. F. M., Tielens A. G. G. M., Barlow M. J., 2002, A&A, 382, 184
Natta A., Hollenbach D., 1998, A&A, 337, 517
Palla F., Brand J. Cesaroni R., Comoretto G., Felli M., 1991, A&A, 246, 249
Parker Q. A. et al., 2003, in Kwok S., Dopita M., Sutherland R., eds, IAU Symp. 209, Planetary Nebulae: Their Evolution and Role in the Universe. Astron. Soc. Pac., San Francisco, p. 25
Parker Q. A. et al., 2006, MNRAS, 373, 79
Peimbert M., 1990, Rev. Mex. Astron. Astrofis., 20, 119
Peimbert M., 1993, in Weinberger R., Acker A., eds, IAU Symp. 155, Planetary Nebulae. Kluwer, Dordrecht, p. 523
Perek L., Kohoutek L., 1967, Catalogue of Galactic Planetary Nebulae. Academia Publishing House, Prague
Phillips J. P., 1989, in Torres-Peimbert S., ed., IAU Symp. 131, Planetary Nebulae. Kluwer, Dordrecht, p. 425
Phillips J. P., 2001, PASP, 113, 839
Phillips J. P., 2002, ApJS, 139, 199
Phillips J. P., 2004, Rev. Mex. Astron. Astrofis., 40, 193
Phillips J. P., 2006a, Rev. Mex. Astron. Astrofis., 42, 229
Phillips J. P., 2006b, MNRAS, 368, 819
Phillips J. P., 2007a, MNRAS, 378, 231
Phillips J. P., 2007b, MNRAS, 380, 369
Phillips J. P., 2007c, Rev. Mex. Astron. Astrofis., 43, 303
Phillips J. P., 2007d, New Astron. 13, 60
Phillips J. P., Ramos-Larios G., 2005, MNRAS, 364, 849
Phillips J. P., Ramos-Larios G., 2006, MNRAS, 368, 1773
Phillips J. P., Ramos-Larios G., 2007, AJ, 133, 347
Phillips J. P., Ramos-Larios G., 2008, MNRAS, 383, 1029
Phillips J. P., Mampaso A., Vilchez J. M., Gomez P., 1984, Ap&SS, 122, 81
Pottasch S. R., 1984, Planetary Nebulae. Reidel, Dordrecht
Pottasch S. R., Bignell C., Olling R., Zijlstra A. A., 1988, A&A, 205, 248
Preite-Martinez A., 1988, A&AS, 76, 317
Ramos-Larios G., Phillips J. P., 2005, MNRAS, 357, 732
Ramos-Larios G., Phillips J. P., 2006, Rev. Mex. Astron. Astrofis., 42, 131
Reach W. T. et al., 2005, PASP, 117, 978
Riesgo H., López J. A., 2006, Rev. Mex. Astron. Astrofis., 42, 47
Sabbadin F., Minello S., Bianchini A., 1977, A&A, 60, 147
Schlegel D. J., Finkbeiner D. P., Davis M., 1998, ApJ, 500, 525
Sternberg A., Dalgarno A., 1989, ApJ, 338, 197
Storey J. W. V., 1984, MNRAS, 206, 521
Su K. Y. L. et al., 2004, ApJS, 154, 302
Su K. Y. L. et al., 2007, ApJ, 657, 41
Tielens A. G. G. M., 2005, The Physics and Chemistry of the Interstellar Medium. Cambridge Univ. Press, Cambridge
Ueta T., 2006, ApJ, 650, 228
Volk K., Kwok S., 2003, in Kwok S., Dopita M., Sutherland R., eds, Proc. IAU Symp. 209, Planetary Nebulae: Their Evolution and Role in the Universe. Astron. Soc. Pac., San Francisco, p. 303
Werner M. et al., 2004, ApJS, 154, 1
Whitney B. A., Wood K., Bjorkman J. E., Cohen M., 2003, ApJ, 598, 1079
Zijlstra A. A., Pottasch S. R., 1991, A&A, 243, 478

This paper has been typeset from a MS Word file prepared by the author.